TWO-EQUATION TURBULENCE MODEL FOR FLOW IN TRENCHES

By Ben J. Alfrink[1] and Leo C. van Rijn[1]

ABSTRACT: Steady recirculating flow is described by means of a mathematical model based on the full unsteady Reynolds equations and the k-ϵ model for turbulence closure. The model is applied to the flow in a steep-sided trench perpendicular to the main flow direction. Inlet profiles are taken with reference to developed channel flow. For the wall boundary a local equilibrium is assumed, yielding among others a logarithmic behavior for the mean flow velocity. The constants of the k-ϵ model are related to the roughness conditions. A sensitivity study is reported to identify the relative importance of the various constants and inlet conditions. Numerical results are compared with laboratory experiments.

INTRODUCTION

The design of civil engineering projects such as harbors, traffic tunnels, pipelines, and storm surge barriers often requires the dredging of trenches or channels in the alluvial bed of a river or estuary. To estimate the fluid forces acting on the submerged structures or to compute the siltation rate of a dredged trench, detailed knowledge of the flow and turbulence field is of importance (6). Recent approaches based on mixing length or one-equation (turbulence energy) modeling are still not predictive because the empirical coefficients applied are not shown to be universally applicable (7).

In the present paper, the turbulent flow in a steep-sided trapezoidal trench placed perpendicular to the main flow direction is treated using an advanced mathematical model. The model is based on the full two-dimensional unsteady Reynolds equations for the mean flow. Turbulence closure is obtained by means of a two-equation model consisting of transport equations for the turbulence kinetic energy, k, and its dissipation rate, ϵ. To handle arbitrary geometries, general boundary fitted curvilinear coordinates are used.

The constants of the k-ϵ model are related to the roughness conditions. An extensive study is reported to identify the relative importance of the various constants and inlet conditions. Computational results are compared with laboratory experiments.

Basic Equations and Assumptions.—The mathematical description of the flow model is based on the time averaged equations of motion and continuity stating conservation of momentum and mass:

$$\frac{\partial \bar{v}_i}{\partial t} + \bar{v}_j \frac{\partial \bar{v}_i}{\partial x_j} + \frac{1}{\rho}\frac{\partial \bar{p}}{\partial x_i} - \frac{1}{\rho}\frac{\partial \tau_{ij}}{\partial x_j} = \bar{f}_i \quad \ldots\ldots\ldots\ldots\ldots\ldots\ldots\ldots\ldots\ldots\ldots\ldots\ldots\ldots (1)$$

[1]Project Engrs., Delft Hydraulics Lab., De Voorst Lab., Postbox 152, Emmeloord, The Netherlands.

Note.—Discussion open until December 1, 1983. To extend the closing date one month, a written request must be filed with the ASCE Manager of Technical and Professional Publications. The manuscript for this paper was submitted for review and possible publication on October 8, 1982. This paper is part of the Journal of Professional Issues in Engineering, Vol. 109, No. 3, July, 1983. ©ASCE, ISSN 0733-9429/83/0007-0941/$01.00. Paper No. 18094.

$$\frac{\partial \bar{v}_i}{\partial x_i} = 0 \quad \ldots\ldots (2)$$

in which x_i = Cartesian coordinates; $\bar{v}_i$ = velocity components in x_i-direction; t = time; $\bar{p}$ = pressure; ρ = density of the fluid; τ_{ij} = Reynolds stresses; and $\bar{f}_i$ = components of external forces per unit of mass in x_i-direction. Einstein's summation convention has been applied.

The Reynolds stresses, τ_{ij}, are defined by

$$\tau_{ij} = \rho \nu \left(\frac{\partial \bar{v}_i}{\partial x_j} + \frac{\partial \bar{v}_j}{\partial x_i} \right) - \rho \overline{v_i' v_j'} \quad \ldots\ldots (3)$$

in which the prime denotes the fluctuating part, and ν = kinematic viscosity.

Turbulence closure will be obtained by means of a two-equation model consisting of transport equations for the turbulence kinetic energy per unit of mass k:

$$k = \frac{1}{2} \overline{v_i' v_i'} \quad \ldots\ldots (4)$$

and its dissipation rate ϵ:

$$\epsilon = \nu \overline{\frac{\partial v_i'}{\partial x_j} \frac{\partial v_i'}{\partial x_j}} \quad \ldots\ldots (5)$$

The framework of the k-ϵ turbulence model is based on Boussinesq's hypothesis, in which the stresses, $-\rho \overline{v_i' v_j'}$, are approximated in a way analogous to the expression for the viscous stresses:

$$-\overline{v_i' v_j'} = \nu_t \left(\frac{\partial \bar{v}_i}{\partial x_j} + \frac{\partial \bar{v}_j}{\partial x_i} \right) - \frac{2}{3} k \delta_{ij} \quad \ldots\ldots (6)$$

in which δ_{ij} = Kronecker delta function.

It can be assumed that the eddy viscosity, ν_t, is proportional to a velocity scale and a length scale characterizing the (large-scale) turbulent motion. In terms of k and ϵ, this yields the Kolmogorov-Prandtl expression in the following form:

$$\nu_t = c_\mu \frac{k^2}{\epsilon} \quad \ldots\ldots (7)$$

in which c_μ = a constant.

The transport equations of the standard k-ϵ model (13) finally read as

$$\frac{\partial k}{\partial t} + \bar{v}_i \frac{\partial k}{\partial x_i} - \frac{\partial}{\partial x_i} \left(\frac{\nu_t}{\sigma_k} \frac{\partial k}{\partial x_i} \right) = \nu_t \left(\frac{\partial \bar{v}_i}{\partial x_j} + \frac{\partial \bar{v}_j}{\partial x_i} \right) \frac{\partial \bar{v}_i}{\partial x_j} - \epsilon \quad \ldots\ldots (8)$$

$$\frac{\partial \epsilon}{\partial t} + \bar{v}_i \frac{\partial \epsilon}{\partial x_i} - \frac{\partial}{\partial x_i} \left(\frac{\nu_t}{\sigma_\epsilon} \frac{\partial \epsilon}{\partial x_i} \right) = c_1 \frac{\epsilon}{k} \nu_t \left(\frac{\partial \bar{v}_i}{2 x_j} + \frac{\partial \bar{v}_j}{\partial x_i} \right) \frac{\partial \bar{v}_i}{\partial x_j} - c_2 \frac{\epsilon^2}{k} \quad \ldots\ldots (9)$$

in which the kinematic viscosity has been neglected against the eddy viscosity. The right-hand members describe production by shear and dissipation (destruction), respectively.

The k-ϵ model thus implies the use of five constants: c_μ, c_1, c_2, σ_k, and σ_ϵ. The determination of the constants is analyzed in the following.

Boundary Conditions.—In the present study, the following boundary types are distinguished: bottom, free surface, inlet, and outlet boundaries.

Bottom Boundary.—For fully rough flow ($v_* k_s/\nu > 60$) computations are possible down to a level, z_o, in which the velocity is zero according to the logarithmic profile

$$\frac{\bar{v}_s}{v_*} = \frac{1}{\kappa} \ln \frac{z}{z_o} \quad \ldots\ldots (10)$$

in which $\bar{v}_s$ = flow velocity parallel to bottom; v_* = shear velocity at the bottom; κ = Von Kármán constant; z = distance from bottom; z_o = zero velocity level (= 0.033 k_s); and k_s = equivalent roughness height of the grains. Equation 10 is valid for the near bottom region, which is approximately 0.1–0.2 times the water depth.

Discretization problems will arise when the no-slip condition

$$\bar{v}_n = \bar{v}_s = 0 \quad \ldots\ldots (11)$$

is applied, due to the large velocity gradients that occur close to the bottom. Therefore, the grid ends at some distance from the bottom where the velocity gradients are relatively smaller. It is then assumed that the velocity component normal to the bottom vanishes:

$$\bar{v}_n = 0 \quad \ldots\ldots (12)$$

while the tangential shear is computed from the logarithmic profile, Eq. 10:

$$\frac{\partial \bar{v}_s}{\partial n} = \frac{v_*}{\kappa z} \quad \ldots\ldots (13)$$

The following set of boundary conditions for κ and ϵ (13) is used:

$$k = \frac{v_*^2}{c_\mu^{0.5}} \quad \ldots\ldots (14)$$

$$\epsilon = \frac{|v_*|^3}{\kappa z} \quad \ldots\ldots (15)$$

Free Surface Boundary.—A rigid-lid approximation is made, in which the free surface is replaced by a fixed (free-slip) boundary on which a nonzero pressure may result. The latter is a measure of the surface elevation which could occur if the surface were free. This assumption appears to be valid for low Froude numbers. The formulas read [$\bar{v}_n = 0$ (Eq. 12)]:

$$\tau_{sn} = \rho \nu_t \left(\frac{\partial \bar{v}_n}{\partial s} + \frac{\partial \bar{v}_s}{\partial n} \right) = 0 \quad \ldots\ldots (16)$$

The latter condition results in a symmetry condition

$$\frac{\partial \bar{v}_s}{\partial n} = 0 \quad \ldots\ldots (17)$$

when the impermeable wall condition, Eq. 12, is used. For the scalar turbulence variables, k and ϵ, the symmetry condition applies as well:

$$\frac{\partial k}{\partial n} = \frac{\partial \epsilon}{\partial n} = 0 \quad \text{(18)}$$

Inlet Boundary.—At the inlet, velocity components and turbulence variables are prescribed using the standard formulas for open channel flow:

$$\bar{v}_s = 0 \quad \text{(19)}$$

$$\frac{\bar{v}_n}{v_*} = \frac{1}{\kappa} \ln \frac{z}{z_o} \quad \text{(20)}$$

$$k = \frac{v_*^2}{c_\mu^{0.5}} \left(1 - \frac{z}{H}\right) \quad \text{(21)}$$

$$\epsilon = \frac{|v_*|^3}{\kappa z} \left(1 - \frac{z}{H}\right) \quad \text{(22)}$$

in which $\bar{v}_n$ = flow velocity normal to inlet boundary; $\bar{v}_s$ = flow velocity parallel to inlet boundary; H = local flow depth. Equations 21–22 are coherent with the bottom boundary conditions, Eqs. 14–15. The inlet profiles correspond with the bottom boundary conditions for $z << H$. Equation 22 has been derived from the eddy viscosity distribution

$$\nu_t = \kappa v_* z \left(1 - \frac{z}{H}\right) \quad \text{(23)}$$

and Eqs. 7 and 21.

Outlet Boundary.—Taking the outlet far enough away from the region of interest, it can be assumed that convection is dominating. Boundary values for the velocity components are determined from upstream events by means of the method of characteristics. Normal derivatives of k and ϵ along the outlet boundary are set to zero.

Finite Difference Approximation.—The numerical method is based on the use of curvilinear finite differences in space and of fractional steps in time. Convective and diffusive transports are solved separately. Concerning the equations of motion, the time discretization is similar to the method proposed by Chorin (3).

Time Discretization.—To explain the time-discretization, suppose the velocity is known at time $t = m\,\Delta t$. For ease of notation, the bars denoting turbulence averaged variables will be omitted hereafter.

The new velocity, v_i^{m+1}, is then firstly approximated to an auxiliary velocity, v_i^{aux}, by solving the equations of motion excluding the pressure gradient terms:

$$\text{I} \quad \frac{v_i^{\max} - v_i^m}{\Delta t} = \left\{ -v_j \frac{\partial v_i}{\partial x_j} + \frac{\partial}{\partial x_j} \left[\nu_t \left(\frac{\partial v_i}{\partial x_j} + \frac{\partial v_j}{\partial x_i} \right) \right] \right\}_m^{\text{aux}} \quad \text{(24)}$$

This auxiliary velocity contains the correct vorticity but has nonzero divergence. So it has to be modified in such a way as to preserve the

vorticity but to bring the divergence to zero. This is accomplished by solving the complementary system

$$\text{II}\begin{cases}\dfrac{v_i^{m+1}-v_i^{\text{aux}}}{\Delta t}=-\dfrac{\partial\phi^{m+1}}{\partial x_i} & \text{(25)}\\[2ex] \dfrac{\partial v_i^{m+1}}{\partial x_i}=0 & \text{(26)}\end{cases}$$

in which ϕ = a virtual pressure, defined by

$$\phi=\frac{p}{\rho}+\frac{2}{3}k+g\,x_3 \quad \text{(27)}$$

in which x_3 = vertical coordinate. The $-2/3\ k\ \delta_{ij}$ contributions of the Reynolds stresses have been combined with the pressure, p. In addition, the hydrostatic part of the pressure has been eliminated.

The final velocity field, v_i^{m+1}, is obtained by adding to v_i^{aux} the dynamical effect of the "pressure," ϕ^{m+1}, determined so that the incompressibility condition, Eq. 26, remains satisfied.

Taking the divergence of Eq. 25, and demanding the new velocity to satisfy the equation of continuity, yields a Poisson equation for the pressure:

$$\frac{\partial^2\phi^{m+1}}{\partial x_i\partial x_i}=\frac{1}{\Delta t}\left(\frac{\partial v_i^{\text{aux}}}{\partial x_i}\right) \quad \text{(28)}$$

For the solution of Eq. 28 a boundary condition is necessary; again using Eq. 25, the following Neumann condition results:

$$\frac{\partial\phi^{m+1}}{\partial n}=\frac{1}{\Delta t}\left(v_n^{\text{aux}}-v_n^{m+1}\right) \quad \text{(29)}$$

After the determination of the new pressure field via the solution of Eqs. 28–29, the final velocity, v_i^{m+1}, is calculated explicitly with Eq. 25.

For the solution of Eq. 24, convective and diffusive contributions are considered separately. The nonlinear convective transport is treated explicitly by means of a method of characteristics:

$$\frac{\tilde{v}_i-v_i^m}{\Delta t}=-v_j^m\frac{\partial v_i^m}{\partial x_j} \quad \text{(30)}$$

As turbulent flow is considered, diffusive transports will be important, and to avoid severe stability criteria the equation is solved implicitly:

$$\frac{v_i^{\text{aux}}-\tilde{v}_i}{\Delta t}=\frac{\partial}{\partial x_j}\left[\nu_t\left(\frac{\partial v_i^{\text{aux}}}{\partial x_j}+\frac{\partial v_j^{\text{aux}}}{\partial x_i}\right)\right] \quad \text{(31)}$$

Consider next the transport equations for the turbulence variables k and ϵ. Apart from the pressure gradient terms, Eqs. 8–9 are seen to have the same structure as the equations of motion. The convective and diffusive transports are again treated separately, in which the same methods of solution can be used as for the equations of motion. A description

of the methods of solution is given in Appendix I.

Curvilinear Coordinates.—In finite difference techniques, one practical way of treating boundary conditions that are specified along an arbitrary curve is to map the boundary curve onto a grid coordinate line. In this way finite difference methods become more powerful and accurate.

In considering the trench geometry of the present application (Fig. 1), a coordinate transformation has been used which is of a simple analytical nature. In the vertical direction, a stretching of coordinates to the wall is applied.

The coordinate transformation yields a nonorthogonal grid and shows some discontinuities. But although nonorthogonal grids complicate the form of the differential equations—introducing cross-derivatives—they do not essentially affect the band width of equation matrices, nor do they change the character of the equations.

Constants.—The k-ϵ model implies the use of five constants: c_μ, c_1, c_2, σ_k, and σ_ϵ. Some of the constants are correlated, as can be seen by assuming a local energy equilibrium in the near wall region where a logarithmic velocity distribution prevails. Assuming equal production and dissipation of turbulence energy, k, and neglecting the convection of ϵ, the transport equation for ϵ, Eq. 9, reduces (13) to

$$c_1 = c_2 - \frac{\kappa^2}{\sigma_\epsilon c_\mu^{0.5}} \quad \ldots\ldots\ldots\

TABLE 1.—Constants

C_μ (1)	C_1 (2)	C_2 (3)	σ_k (4)	σ_ϵ (5)	κ (6)	References (6)
0.09	1.44	1.92	1.0	1.30	0.435	Launder and Spalding (8)
0.09	1.45	1.90	1.0	1.30	0.42	Pope (10)
0.09	1.44	1.92	1.0	1.11	0.40	Singhal and Spalding (14)

for cubes and gravel. Pyle and Novak (11) even obtained κ-values in the range 0.2–0.3 for spheres and hemispheres with concentrations in the range 20%–80%. Considering the present application, the κ-value is expected to be in the range 0.3–0.4.

Application.—*Experimental Conditions*: To verify the numerical model, laboratory experiments concerning the steady flow in a steep-sided trapezoidal trench placed perpendicular to the main flow direction have been considered (4). The measurements have been carried out in a flume (length = 17 m, depth = 0.7 m, and width = 0.5 m) of the Delft Hydraulics Laboratory. The dimensions of the trench and the upstream hydraulic conditions have been varied, F being in the range 0.2–0.3. A layer of gravel has been used for bed roughness. A Laser Doppler velocity meter has been used to determine the longitudinal and vertical mean flow velocities, the root-mean-square values (turbulence intensities) of the turbulent flow velocity fluctuations, and the turbulent shear stresses. All measurements have been made in the center line of the flume, with a measuring time of 200 sec.

In the present paper, attention will be focused on one representative experiment (T8). The application of the model for the other experiments is described in Ref. 12; the geometrical description is given in Fig. 1, together with the location of the measuring stations. The average height of the gravel particles on the flume bottom was about 0.006 m, and the equivalent roughness height, k_s, was found to be about 0.02 m and thus $z_o = 0.00067$ m.

As the flow velocity profile at the inlet boundary ($x = 0$) is described by Eq. 20, the bed-shear velocity, v_*, the constant of Von Karman, κ, and the equivalent roughness of Nikuradse, k_s, must be specified. Two methods have been used to determine the v_*, κ, and k_s-parameters:

1. Assuming the k_s-parameter (= 0.02 m) and the κ-parameter (= 0.4 or 0.35) to be known and fitting with the measured flow velocity profile at the inlet boundary resulting in the v_*-values for the computations 1–4 (Table 2).
2. Assuming the κ-parameter to be known only (0.435, 0.40, or 0.35) and fitting with the measured flow velocity profile resulting in the v_*- and z_o-values for the computations 5–11 (Table 2).

Table 2 summarizes the input data and constants as well as some computational results concerning the location of the separation point and the reattachment point with regard to station 2 (Fig. 1). It is remarked that the shear velocity at the bottom is specified at the inlet boundary only. At the other locations this value is computed by means of the model.

TABLE 2.—Input Data, Constants, and Computational Results

Number (1)	Input Data: v_*, in meters per second at $x = 0$ (2)	Input Data: z_o, in meters (3)	Constants: κ (4)	Constants: c_μ (5)	Constants: c_1 (6)	Constants: c_2 (7)	Constants: σ_k (8)	Constants: σ_ϵ (9)	Constants: c_k (10)	Computational Results: x_s, in meters (11)	Computational Results: x_r, in meters (12)
1	0.0330	0.00067	0.40	0.09	1.51	1.92	1.0	1.30	1.0	0.100	0.95
2	—	—	—	—	—	—	—	—	0.67	0.100	1.00
3	—	—	—	0.20	1.65	—	—	—	1.0	0.100	1.05
4	0.0290	—	0.35	0.09	1.60	—	—	—	—	0.100	1.25
5	0.0473	0.0022	0.435	0.09	1.44	1.92	1.0	1.30	1.0	0.100	0.85
6	0.0435	—	0.40	—	1.51	—	—	—	—	0.075	1.05
7	0.0380	—	0.35	—	1.60	—	—	—	—	0.075	1.35
8	0.0435	0.0022	0.40	0.09	1.60	1.92	1.0	1.30	1.0	0.075	1.25
9	0.0380	—	0.35	—	1.51	—	—	—	—	0.075	1.10
10	0.0380	0.0022	0.35	0.09	1.44	1.75	1.0	1.30	1.0	0.050	1.30
11	0.0380	0.0022	0.35	0.09	1.44	1.92	1.0	0.85	1.0	0.075	0.90
	measured reattachment point										1.45

The most important features of the various computations will now be described.

Influence of Flow Velocity Profile at Inlet.—The influence of the flow velocity profile at the inlet boundary on the computed flow and turbulence field in the trench can be investigated by comparing computations 1 and 6 (or 4 and 7) because in these computations all turbulence constants are held the same.

As can be seen from Table 2, the values for the separation and reattachment length according to the computations 6 (and 7) are only slightly larger than according to the computations 1 (and 4). Therefore, the flow velocity profile at the inlet boundary does not seem to influence importantly the computed flow field in the trench.

Influence of Turbulence Energy Profile at Inlet.—To analyze the influence of the turbulence energy profile at the inlet boundary, an additional constant, c_k, is introduced and Eqs. 21–22 are replaced by

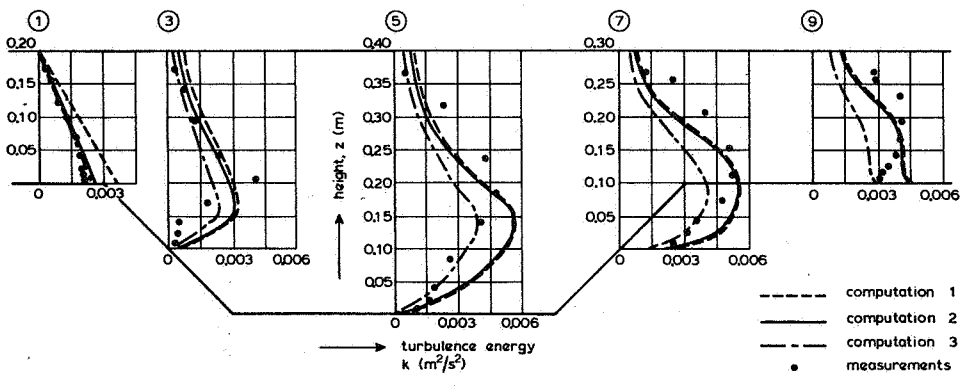

FIG. 2.—Turbulence Energy Profiles

$$k = c_k \frac{v_*^2}{c_\mu^{0.5}} \left(1 - \frac{z}{H}\right) \quad \text{(33)}$$

$$\epsilon = c_k^2 \frac{|v_*|^3}{\kappa z} \left(1 - \frac{z}{H}\right) \quad \text{(34)}$$

Computations 1 and 2, in which the c_k-constant has been varied, can be used to show the influence of the turbulence energy profile at the inlet on the computed turbulence energy field in the trench. Figure 2 shows the computed k-profiles at stations 1, 3, 5, 7, and 9. Although at the inlet boundary a noticeable difference (50%) is introduced, the differences at station 5 are already negligible. At the inlet boundary, computation 2 gives the best agreement with measured values. The measured values were estimated from the measured turbulence intensities $(\hat{u}, \hat{w})$ by taking $\hat{v}^2 = \hat{w}^2$:

$$k = 0.5(\hat{u}^2 + 2\hat{w}^2) \quad \text{(35)}$$

in which $\hat{u} = [\overline{(u')^2}]^{0.5}$ (36*a*)

and $\hat{w} = [\overline{(w')^2}]^{0.5}$ (36*b*)

The computed flow velocities in computations 1 and 2 are almost identical. Therefore, it seems that accurate information for the turbulence energy profile, and thus the dissipation rate at the inlet boundary, is not of major importance.

Influence of c_μ and c_1-Constants.—In computation 3, a c_μ-constant equal to 0.2 has been used. In this way an optimal agreement between the measured and computed turbulence energy profiles at the inlet boundary is obtained without use of the c_k-constant (Fig. 2). Equation 32 has been used to modify the c_1-constant. Although the modifications have a noticeable influence on the computed turbulence energy profiles (Fig. 2), the influence on the computed mean flow velocity, shear stress, and eddy viscosity profiles is negligibly small (not shown). So it does not seem necessary to change the standard value of the c_μ-constant (= 0.09) as proposed by Launder and Spalding (8), even if measurements of the turbulence energy at the inlet indicate a significantly different value.

Influence of κ- and c_1-Constants.—Computations 1 and 4 show the combined influence of the κ and the c_1-constants. By assuming $\kappa = 0.35$ instead of $\kappa = 0.40$, the c_1-constant changes from 1.51 to 1.60 according to Eq. 32. The ratio of v_* and κ is kept constant to obtain the same flow velocity profile at the inlet boundary. Apart from the changed κ and c_1-constants, computations 1 and 4 are identical. However, the recirculation length shows an increase of about 30% (Table 3).

Also, computations 5, 6, and 7 show the influence of the κ and c_1-constants. It may be noted that the constants in computation 5 are equal to those suggested by Launder and Spalding. The results of computations 5 and 7 are shown in Table 3 and Fig. 3. As can be observed, computation 7 yields the best agreement between measured and computed flow velocities, although the agreement is still not optimal. However, it must be remarked that the experiments show serious three-dimensional effects, probably due to the limited flume width (= 0.5 m).

TABLE 3.—Influence of Constants on Recirculation Length

Computations (1)	κ (2)	c_1 (3)	c_2 (4)	σ_ϵ (5)	Recirculation length (6)
1 and 4	−10%	+5%			+30%
5 and 7	−20%	+10%			+60%
6 and 7	−10%	+5%			+30%
6 and 9	−10%				+5%
8 and 7	−10%				+10%
9 and 7		+5%			+25%
6 and 8		+5%			+20%
5 and 10	−20%		−10%		+50%
5 and 11	−20%			−35%	+5%

This can be demonstrated by computing the discharge in the center line of the flume. For example, in station 3 the "measured" discharge per unit of width is 0.076 m^2/s, while in station 1 a value of 0.082 m^2/s is observed.

With regards to the turbulence-energy profiles, computation 7 also produces the best results. Apart from station 1 and 9, the agreement is quite satisfactory. With regard to the shear-stress profiles, the results of computation 7 are less good. The adjustment of the computed values proceeds too slowly compared with measured values. The deviations are still noticeable at the downstream section where the computed shear stresses are too low.

Apparently, the choice of the κ-constant and, thus, the c_1-constant is important. Both constants influence the eddy viscosity, either directly or indirectly. Reducing the κ-constant results in a reduction of the eddy viscosity at the inlet, and the c_1-constant influences the eddy viscosity through the k-ϵ equations.

To identify which of the two constants has a dominating effect, the c_1-constant has been changed in computations 9 and 7 and also in computations 6 and 8. In these four computations, both the flow velocity and eddy viscosity profiles at the inlet are identical. However, it must be remarked that Eq. 32 is not satisfied for computations 8 and 9. Considering the recirculation length (Table 3), the c_1-constant seems to be important, as a change of about 5% in the c_1-constant results in a change of about 20% in the recirculation length. A similar influence has been reported by Rodi (13) for the spreading rate of a jet.

Comparison of computations 6 and 9 (and also 8 and 7) shows a less significant influence of the κ-constant: a maximum increase of the recirculation length of 10% for a reduction of the κ-constant by about 10% (Table 3). This result seems to disagree with the results of Pope (10) who reported an increase of the recirculation length by about 25% when the κ-constant decreases by 10%. However, as Pope's description is rather brief, it is not clear whether the constants were varied in a coherent manner.

Influence of c_2-Constant.—In computation 10, the c_2-constant is adjusted using the reversed version of Eq. 32. Assuming $\kappa = 0.35$ and the c_μ, c_1, and σ_ϵ-constants equal to the values proposed by Launder and

Spalding, the c_2-constant will be equal to 1.75. Compared with computation 7, the results are nearly identical. Compared with computation 5, the κ-constant decreases by about 20% and the c_2-constant by about 10%, but the recirculation length increases with more than 50%! Consequently, the sensitivity of the computation for the c_2-constant seems to be similar to the sensitivity for the c_1-constant (see also Table 3, computations 5 and 10, computations 5 and 7), and again similar to the data reported by Rodi.

Influence of σ_ϵ-Constant.—In computation 11, the σ_ϵ-constant was adjusted by applying Eq. 32, assuming $\kappa = 0.35$ resulting in $\sigma_\epsilon = 0.85$. A similar modification has been done by Singhal and Spalding (14). Comparing computations 5 and 11 (Table 2) it can be observed that the recirculation length is hardly changed. Therefore, it can be concluded that the influence of σ_ϵ is negligibly small.

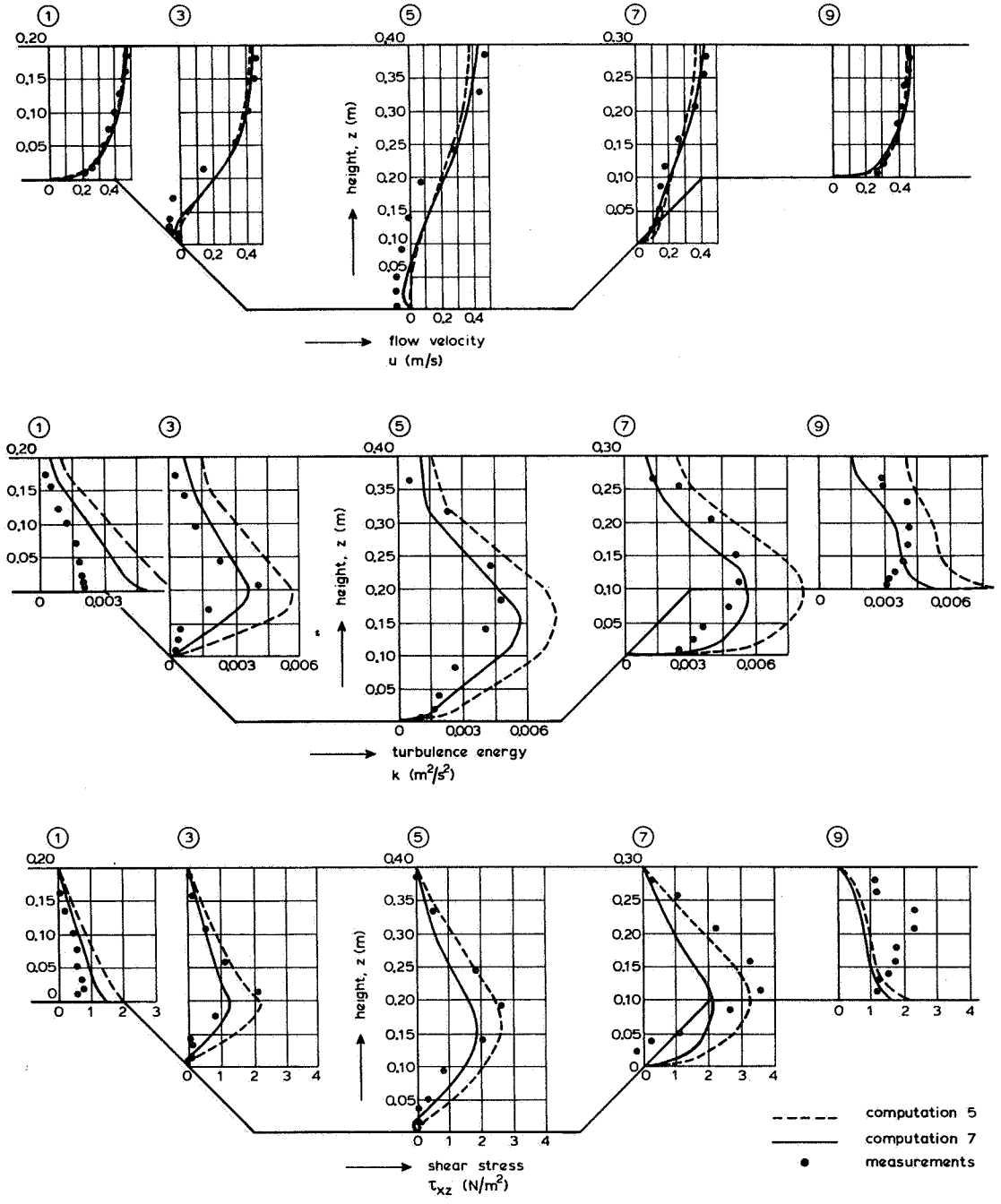

FIG. 3.—Flow Velocity, Turbulence Energy, and Shear Stress Profiles

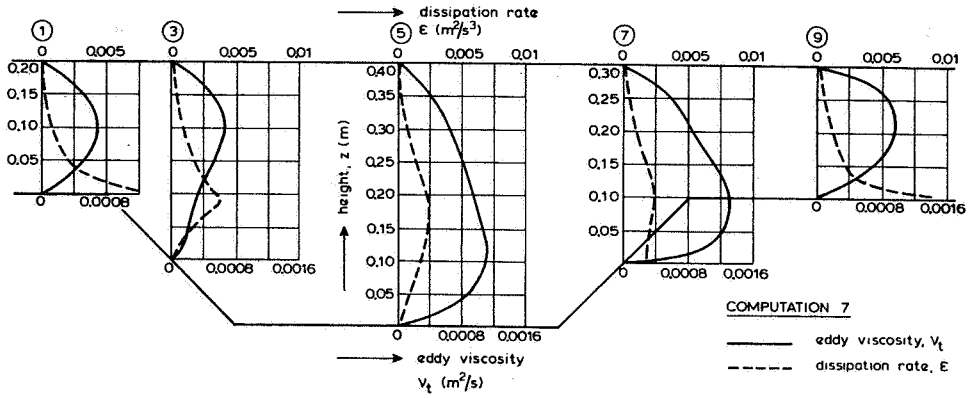

FIG. 4.—Eddy Viscosity and Dissipation Rate Profiles

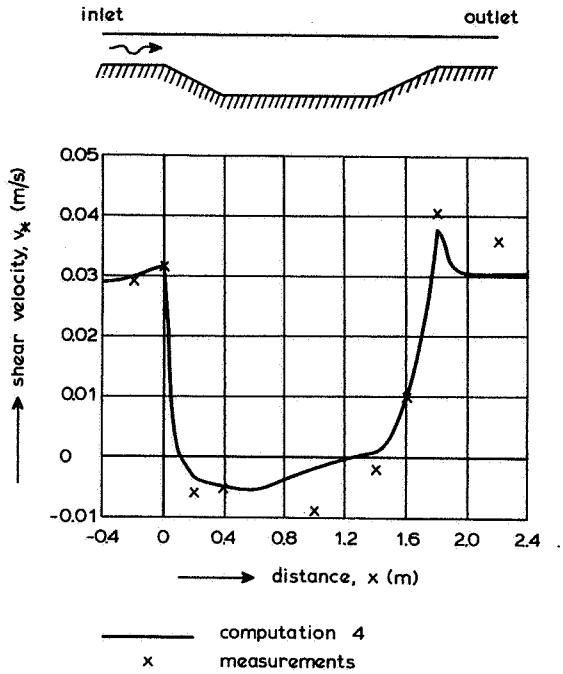

FIG. 5.—Measured and Computed Shear Velocities

Finally, some additional computational results are presented. Figure 4 shows the computed eddy viscosity and dissipation rate profiles for computation 7, and Fig. 5 presents "measured" and computed shear velocities at the bottom boundary. The "measured" values were computed from the flow velocities measured at the lowest measuring points using Eq. 10, with $k_s = 0.02$ m and $\kappa = 0.35$.

Computational Details.—In general, time steps ranging between 0.05 and 0.1 sec are sufficient to yield stable and accurate results. This agrees with a Courant number less than unity (Eq. 43). A further reduction of the time step does not give an improvement.

The steady state can be considered to be reached after 30 sec physical time. One time step for the (56 × 11) grid of Fig. 1 takes less than 1 sec CPU time on an IBM 3033 computer. The core memory is restricted to 500 K bytes.

In the vertical direction, 11 grid points have been taken using a coordinate stretching towards the wall. The grid has been refined locally in the horizontal direction around the expected point of separation. A further reduction of the grid size does not give an improvement.

Apart from the local grid refinement, no specific measures have been taken around expected points of separation and reattachment, e.g., compare with Ref. 15.

Conclusions

The following conclusions can be made:

1. Steady recirculating flow can be predicted reasonably well by means of a mathematical model based on the full Reynolds equations and a k-ϵ model for turbulence closure.
2. The constants of the k-ϵ model are related to the roughness conditions using Eq. 32.
3. Accurate data for the flow velocity profile at the inlet boundary are of minor importance.
4. Accurate turbulent energy and dissipation rate profiles at the inlet are of minor importance.
5. The computational results are most sensitive to changes in the κ-constant in combination with the c_1- or c_2-constant, the latter being dominant.
6. The sensitivity of the results to changes in the σ_ϵ-constant is negligibly small.

Acknowledgment

The work reported in this paper was carried out while the first writer was a visiting scientist in the "Laboratoire National d'Hydraulique," a department of the "Electricité de France," Chatou, France. He would like to thank J. P. Benqué, O. Daubert, and P. L. Viollet for many stimulating discussions. Use has been made of existing computer programmes and facilities of Electricité de France.

Appendix I.—Description of Methods of Solution

Convective Transport.—The transport equation to be solved can be written generally as

$$\frac{\partial f}{\partial t} + v_i \frac{\partial f}{\partial x_i} = 0 \quad \ldots\ldots (37)$$

in which the velocity, v_i, is supposed to be known. The scalar $f = v_i$, k, and ϵ, respectively. For two-dimensional flow in the vertical plane, Eq. 37 can be written as

$$\frac{\partial f}{\partial t} + u \frac{\partial f}{\partial x} + w \frac{\partial f}{\partial z} = 0 \quad \ldots\ldots (38)$$

The character of Eq. 38 is strictly hyperbolic; the equation can be solved successfully with a method of characteristics. For computational reasons, another splitting has been applied in order to reduce the space dimension. Due to the use of curvilinear coordinates the fractional steps read

$$\frac{\partial f}{\partial t} + u^* \frac{\partial f}{\partial \xi} = 0 \quad \ldots\ldots (39a)$$

and $$\frac{\partial f}{\partial t} + w^* \frac{\partial f}{\partial \eta} = 0 \quad \ldots\ldots (39b)$$

in which $$u^* = u \frac{\partial \xi}{\partial x} + w \frac{\partial \xi}{\partial z} \quad \ldots\ldots (40a)$$

$$w^* = u \frac{\partial \eta}{\partial x} + w \frac{\partial \eta}{\partial z} \quad \ldots\ldots (40b)$$

ξ and η = the new curvilinear coordinates. The solution of Eq. 39*a* proceeds in the following way: If f is to be computed at the node M, the trajectory (characteristic curve) issuing from M is drawn (Fig. 6), using

$$\frac{d\xi}{dt} = u^* \quad \ldots\ldots (41)$$

for $m\,\Delta t \le t \le (m+1)\Delta t$, with a linear interpolation of u^* inside a mesh. The transport Eq. 39*a* expresses that f is constant along the trajectory, so

$$f(M) = f(N) \quad \ldots\ldots (42)$$

The value $f(N)$ is interpolated from the values of f at surrounding nodes, using a third-order polynomial, which may be reduced to a linear interpolation in order to avoid parasitic oscillations.

The method is unconditionally stable in each direction. However, due to the splitting of coordinates, the Courant conditions

$$C_\xi = u^* \frac{\Delta t}{\Delta \xi} < 1 \quad \ldots\ldots (43a)$$

$$C_\eta = w^* \frac{\Delta t}{\Delta \eta} < 1 \quad \ldots\ldots (43b)$$

have to be satisfied in order to preserve an accurate solution (16). Recently, the same method without splitting became available (5). Both variants yield the same results when the Courant conditions are satisfied.

Diffusive Transport.—The fractional diffusion step is approximated by means of parabolic equation

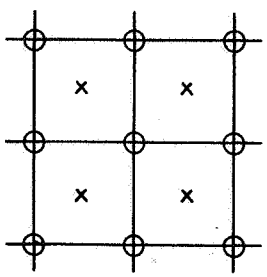

FIG. 6.—Characteristic Curve in (ξ, t)-Plane

$$\frac{\partial f}{\partial t} = \frac{\partial}{\partial x_i}\left(a\frac{\partial f}{\partial x_i}\right) \quad \ldots\ldots (44)$$

in which $a = \nu_t$ $\ldots\ldots (45a)$

for $f = v_i \quad a = \dfrac{\nu_t}{\sigma_k}$ $\ldots\ldots (45b)$

for $f = k$, and $a = \dfrac{\nu_t}{\sigma_\epsilon}$ $\ldots\ldots (45c)$

for $f = \epsilon$. In order to avoid severe stability criteria, Eq. 44 is treated implicitly. Reduction of the space-dimension by means of another time splitting is not meaningfully possible, as cross-derivatives occur due to the nonorthogonal grid.

The discretization of the right-hand member of Eq. 44 yields, in general, a nine point molecule. The resulting system of algebraic equations is solved by means of a standard successive over-relaxation (SOR) iterative scheme. Neumann-type boundary conditions are eliminated beforehand in order to aid convergence.

Continuity Correction.—The solution of the Neumann problem, stated by Eqs. 28–29, requires careful attention. Care has to be taken to satisfy Gauss' theorem ("compatibility condition") in discrete form. It has been shown earlier (2), that by using a regular grid, i.e., a grid where pressure and velocity nodes coincide, this is not realized in general. Taking the pressure nodes staggered in space (Fig. 7), the compatibility condition is satisfied exactly without imposing specific boundary conditions for the pressure.

For the moment, boundary conditions for v_n^{aux} and v_n^{m+1} are taken as equal:

$$v_n^{\text{aux}} = v_n^{m+1} \quad \ldots\ldots (46)$$

resulting via Eq. 29 in a homogeneous Neumann condition:

$$\frac{\partial \phi^{m+1}}{\partial n} = 0 \quad \ldots\ldots (47)$$

The tangential component of v_i^{aux} is specified by means of

$$v_s^{\text{aux}} = v_s^{m+1} + \Delta t \frac{\partial \phi^m}{\partial s} \quad \ldots\ldots (48)$$

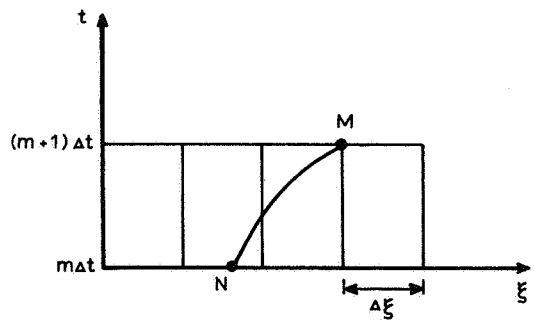

FIG. 7.—Space-Staggered Grid $(o, : v_i, x : \phi)$

Eq. 48 is used to calculate the right-hand member of Eq. 28 on the boundary. Equations 46 and 48 serve as boundary conditions for the diffusion step.

The elliptic operator, appearing in Eq. 28, yields again a nine point molecule. The solution of the resulting system of algebraic equations has been obtained by means of Gaussian elimination with partial pivoting.

Nonlinear Source Terms.—The nonlinear source terms appearing in the transport equations for k and ϵ are treated between the convective and diffusive transport calculations. The equations to be solved read

$$\frac{\partial k}{\partial t} = P - \epsilon \quad \text{(49)}$$

$$\frac{\partial \epsilon}{\partial t} = c_1 \frac{\epsilon}{k} P - c_2 \frac{\epsilon^2}{k} \quad \text{(50)}$$

in which $$P = \nu_t \left(\frac{\partial v_i}{\partial x_j} + \frac{\partial v_j}{\partial x_i} \right) \frac{\partial v_i}{\partial x_j} \quad \text{(51)}$$

They represent a system of coupled, nonlinear, differential equations. The solution is obtained by means of a Runge-Kutta method of fourth order.

Appendix II.—References

1. Alfrink, B. J., "The Computation of Turbulent Recirculating Flow using Curvilinear Finite Differences; Application of the k-ϵ Model to the Flow in Dredged Trenches," *Rapport HE/41/81.22*, Electricité de France, Chatou, France, Aug., 1981.
2. Alfrink, B. J., "On the Neumann Problem for the Pressure in a Navier-Stokes Model," *Proceedings of the International Conference on Numerical Methods in Laminar and Turbulent Flow*, C. Taylor and B. A. Schrefler, eds., Pineridge Press, July, 1981, pp. 389–399.
3. Chorin, A. J., "Numerical Solution of the Navier-Stokes Equations," *Mathematics of Computation*, Vol. 22, 1968, pp. 745–762.
4. "Computation of Siltation in Dredged Trenches, Semi-Empirical Model for the Flow in Dredged Trenches," *Report R 1267-III/M 1536*, Delft Hydraulics Laboratory, Delft, The Netherlands, Nov., 1980.
5. Esposito, P., "Résolution Bi-Dimensionelle des Equations de Transport par la Méthode des Caractéristiques," *Rapport HE/41/81.16*, Electricité de France, Chatou, France, July, 1981.
6. Kerssens, P. J. M., Prins, A., and Rijn, L. C. van, "Model for Suspended Sediment Transport," *Journal of the Hydraulics Division*, ASCE, Vol. 105, No. HY5, Proc. Paper 14574, May, 1979, pp. 461–476.
7. Koutitas, C., and O'Connor, B., "Turbulence Model for Flow over Dredged Trenches," *Journal of the Hydraulics Division*, ASCE, Vol. 107, No. HY8, Proc. Paper 16449, Aug., 1981, pp. 989–1002.
8. Launder, B. E., and Spalding, D. B., "The Numerical Computation of Turbulent Flows," *Computer Methods in Applied Mechanics and Engineering*, Vol. 3, 1974, pp. 269–289.
9. O'Loughlin, E. M., and MacDonald, E. G., "Some Roughness Concentration Effects on Boundary Resistance," *La Houille Blanche*, Vol. 7, Grenoble, France, 1964, pp. 773–783.
10. Pope, S. B., "The Calculation of Separated Boundary Layers," *Proceedings of the Symposium on Turbulent Shear Flows*, Pennsylvania State University, Apr., 1977, pp. 18.35–18.39.

11. Pyle, R., and Novak, P., "Coefficient of Friction in Conduits with Large Roughness," *Journal of Hydraulic Research*, Vol. 19, No. 2, Delft, The Netherlands, 1981, pp. 119–140.
12. Rijn, L. C. van, "The Computation of the Flow and Turbulence Field in Dredged Trenches," *Report S 488-I*, Delft Hydraulics Laboratory, Delft, The Netherlands, 1982.
13. Rodi, W., "Turbulence Models and Their Application in Hydraulics," International Association for Hydraulic Research, Delft, The Netherlands, June, 1980.
14. Singhal, A. K., and Spalding, D. B., "Predictions of Two-Dimensional Boundary Layers with the Aid of the k-ϵ Model of Turbulence," *Computer Methods in Applied Mechanics and Engineering*, Vol. 25, 1981, pp. 365–383.
15. Thomas, C. E., Morgan, K., and Taylor, C., "A Finite Element Analysis of Flow over a Backward Facing Step," *Computers and Fluids*, Vol. 9, Oxford, United Kingdom, 1981, pp. 265–278.
16. Viollet, P. L., Keramsi, A., and Benqué, J. P., "Modélisation Bidimensionelle d'Ecoulements en Charge d'un Fluide Incompressible Non Isotherme," *Journal de Méchanique*, Vol. 20, No. 3, Paris, France, 1981, pp. 557–589.

APPENDIX III.—NOTATION

The following symbols are used in this paper:

a = diffusion coefficient;
c_1, c_2, c_μ = constants in k-ϵ model;
c_k = constant for inlet profile of k;
F = Froude number (= $U/(gH)^{0.5}$);
f = arbitrary scalar function;
f_i = component of external forces per unit of mass in x_i-directions;
g = acceleration due to gravity;
H = local flow depth;
k = kinetic energy of turbulent motion per unit of mass;
k_s = equivalent roughness height of grains;
P = production of kinetic energy;
p = pressure;
t = time;
Δt = integration step in time;
U = upstream flow velocity;
v_i = velocity components in x_i-directions;
v_* = shear velocity at bottom;
x_i = Cartesian coordinates;
z = distance from bottom;
z_o = zero velocity level;
$\Delta\xi\ \Delta\eta$ = integration steps in space;
δ_{ij} = Kronecker delta;
ϵ = dissipation rate of turbulence kinetic energy per unit of mass k;
ξ, η = curvilinear coordinates;
κ = Von Kármán constant;
ν = kinematic viscosity;
ν_t = eddy (turbulent) viscosity;
ρ = density of the fluid;

$\sigma_k, \sigma_\epsilon$ = turbulent Prandtl numbers;
τ_{ij} = components of Reynolds stress tensor; and
Φ = virtual pressure.

Subscripts

n = component in normal direction to local boundary; and
s = component in tangential (parallel) direction to local boundary.

Superscripts

aux = auxiliary variable;
m = time level;
$\tilde{}$ = intermediate time level;
$\bar{}$ = turbulence average; and
$'$ = fluctuating part from turbulence average.